Low Temperature Response of Nanostructured Tungsten Oxide Thin Films towards Hydrogen and Ethanol

M. Ahsan, T. Tesfamichael*, J. Bell*, W. Wlodarski** and N. Motta**

*Faculty of Built Environment and Engineering, Queensland University of Technology, 2 George Street, Brisbane, Queensland 4001, Australia.

**School of Electrical and Computer Engineering, RMIT University, Melbourne, Victoria 3001, Australia.

Corresponding Author: Mohammed Ahsan, School of Engineering Systems, Faculty of BEE, 2 George Street, Brisbane, Queensland 4001, Australia, Email: m.ahsan@qut.edu.au, Phone: 0061731384186, Fax: 0061731381522.

Abstract

Semiconducting metal oxide based gas sensors usually operate in the temperature range 200-500^{o}C. In this paper, we present a new WO_3 thin film based gas sensor for H_2 and C_2H_5OH, operating at 150^{o}C. Nanostructured WO_3 thin films were synthesized by thermal evaporation method. The properties of the as-deposited films were modified by annealing in air at 300^{o}C and 400^{o}C. Various analytical techniques such as AFM, TEM, XPS, XRD and Raman spectroscopy have been employed to characterize their properties. A clear indication from TEM and XRD analysis is that the as-deposited WO_3 films are highly amorphous and no improvement is observed in the crystallinity of the films after annealing at 300^{o}C. Annealing at 400^{o}C significantly improved the crystalline properties of the films with the formation of about 5 nm grains. The films annealed at 300^{o}C show no response to C_2H_5OH (ethanol) and a little response to H_2, with maximum response obtained at 280^{o}C. The films annealed at 400^{o}C show a very good response to H_2 and a moderate response to C_2H_5OH (ethanol) at 150^{o}C. XPS analysis revealed that annealing of the WO_3 thin films at 400^{o}C produces a significant change in stoichiometry, increasing the number of oxygen vacancies in the film, which is highly beneficial for gas sensing. Our results demonstrate that gas sensors with significant performance at low operating temperatures can be obtained by annealing the WO_3 films at 400^{o}C and optimizing the crystalline and nanostructure of the as-deposited films.

Keywords: Tungsten oxide, thin films, gas sensing, thermal evaporation, nanostructured.

1. Introduction

Tungsten oxide (WO_3) is a well-known n-type semiconductor with a band gap of 2.6 -3.6 eV [1, 2], used not only in catalytic/photocatalytic [3] and electrochromic [4] applications but also as solid state gas sensors [4, 5]. Conductometric gas sensors based on the variation of resistivity in thin films are very appealing technologically due to their small size, low cost and low power consumption [5]. The gas sensing performance depends mainly on the method of preparation and resulting microstructure. A number of techniques such as sputtering [6, 7], thermal oxidation [8], thermal evaporation [9], advanced gas deposition [10] and solgel [11] have been used to deposit WO_3 thin films. Each technique has its own advantages and limitations. The sensing properties of the material depend on its microstructure and reactivity of the film surface, as sensors are strongly influenced by presence of oxidizing or reducing gases on the surface. The reactivity is enhanced by presence of defects and adsorbates such as O_2^-, O^{2-} or O^- [12]. The gas sensing properties can be enhanced by reducing the grain size[13], adding impurities[14-17] and modifying the surface morphology and porosity of the films[18]. Inclusion of noble metal impurities such as Au, Ag, Pd or metal oxides such as TiO_2 in WO_3 thin films have shown an improved sensitivity towards various gases [15, 18]. Nanostructures such as In_2O_3 nanowires/nanoneedles and ZnO nanorods have been successfully used to improve sensing performance towards hydrogen [19, 20]. Nanostructured tungsten oxide based conductometric gas sensors have been extensively investigated for H_2S [21], NH_3 [8, 18], NO_x [15, 22-25], O_3 [26], H_2 [27, 28] and ethanol [29-33] detection. WO_3 thin films doped with Pt and Pd have shown a good response to H_2 at 200^{o}C [34, 35]. Iron addition lower than 10 at.% to WO_3 films prepared by reactive RF sputtering produced an enhancement in sensor response when exposed to NO_2 [36]. Improvement in sensing response of WO_3 films to ethanol has also been achieved by reactive rf sputtering process with interruptions [37]. The sensitivity of WO_3 films towards ethanol has been largely attributed to desorption of oxygen at the surface of grains [29-33]. However, as for any other metal oxide based gas sensors, the WO_3 based gas sensors operate efficiently only in the temperature range 200^{o}C-500^{o}C [38]. Recently, there have been lots of attempts to lower the optimum operating temperature of WO_3 based sensors by different fabrication routes [39-41]. For example, deposition techniques such as solgel/calcination and reactive dc magnetron sputtering/annealing have shown a good sensitivity of WO_3 films towards NO_2 at 35^{o}C [42] and 150^{o}C [43] respectively. However, low temperature response of WO_3 thin films prepared by thermal evaporation technique has not been investigated.

The aim of this paper is to investigate the gas sensing performance of thermally evaporated WO_3 thin films at lower operating temperatures towards hydrogen and ethanol. The effect of heat treatment

on the physical, chemical, electronic and gas sensing properties of WO_3 thin films will be analyzed. The film thickness, grain size and purity can be controlled by varying the deposition parameters. Atomic force microscopy (AFM) was used in conjunction with Transmission Electron Microscopy (TEM) to study the surface morphology and grain size. The crystalline properties and phases were determined by XRD and Raman analysis. XPS was used to determine the chemical composition of the films. The gas sensing properties were characterized by using a conductometric gas measurement.

2. Experimental methods

2.1 Sample preparation

Thermal evaporation was used to deposit WO_3 thin films on silica substrate with interdigitated Pt electrodes (Electronics Design Center, Case Western Reserve University, Cleveland, USA). The area of the substrate was 8 mm x 8 mm. The electrode fingers, spaced 100 μm, have a line thickness of 100 μm and a height of 300 nm, respectively. Tungsten oxide (99.9% purity, grain size 20 μm) obtained from Sigma Aldrich Pty Ltd, was used as evaporation source. Before deposition, the powder was placed in desiccator to avoid any moisture and contamination. A bell jar type PVD unit (Varian Coater with AVT Control System, Australia) was used to deposit the WO_3 thin films at a typical pressure of 4×10^{-5} mbar. The substrates were mounted on a substrate holder placed at a distance of 38 cm in line of sight from the evaporation source. The WO_3 thin film deposition was carried out at a rate of 35 nm s^{-1}. A quartz crystal microbalance was used to limit the film thickness to 300 nm. The effect of grain size, porosity, crystallinity and heat treatment for various films with thickness of 300 nm has been measured. The as-deposited films were annealed at 300^{o}C and 400^{o}C for 2 hours in air to improve the microstructural, crystalline and chemical (stoichiometric) properties of the films.

2.2 Sample characterization

A JEOL 1200 TEM at 120 kV was used to investigate the size and shape of WO_3 nanoparticles and crystalline structure of the film. The surface morphology of the films was studied by AFM in semi-contact mode with an NT-MDT P47 Solver Scanning Probe Microscope. The WO_3 film surface was scanned with a silicon tip (radius of curvature 10 nm) over an area ranging from (500 x 500) nm^2 to (2000 x 2000) nm^2. The mean grain size, the grain distribution and the surface roughness were determined by using the Nova NT-MDT Image Analysis Software. XPS analysis was carried out using Kratos AXIS Ultra XPS incorporating a 165 mm hemispherical electron energy analyzer, and using a monochromatic Al Kα source (1486.6 eV) operated at 150 W (15 kV, 15 mA) incident at 45^o with respect to the sample surface, and a line width of 0.2 eV. Photoelectron data were collected at 90^o. Survey scans were taken at 160 eV pass energy and multiple high resolution scans at 20 eV. Survey

scans were carried out over 1200-0 eV binding energy with 1.0 eV steps and a dwell time of 100 ms. Narrow high-resolution scans were run with 0.05 eV steps and 250 ms dwell time. Base pressure in the analysis chamber was 1.3 x 10^{-9} mbar and during sample analysis 1.3 x 10^{-8} mbar. Grazing Incidence X-ray Diffraction (GIXRD) analysis was performed on PANanalytical XPert Pro Multi Purpose Diffractometer (MPD). A Cu K_α radiation of wavelength 1.540 Å was used. The incident angle was kept at 2^o and the 2θ range was kept between 10^o to 85^o with a step size of 0.05^o. Raman measurements were performed using an Oceanoptics QE 6500 spectrometer. A 532 nm line from an argon ion laser was used as the excitation source. To avoid local heating of the samples, a low power of about 5 mW was used. A Raman shift between wavenumbers 200 cm^{-1} and 1200 cm^{-1} has been measured.

2.3 Gas Sensing Measurements

The WO_3 thin film based gas sensors were exposed to H_2 (10-10,000 ppm) and C_2H_5OH (12-185 ppm) in the temperature range 100^oC-280^oC. The gases were diluted in synthetic air to achieve the desired concentrations. For all the experiments, the total flow was adjusted to 200 sccm. The response curve was recorded under a continuous flow of known amount of target gas. A sequence control computer was utilized to computerize the pulse sequence of the target gas concentrations. Initially, synthetic air was passed through the chamber at testing temperature until a stable baseline resistance was observed. Then a sequence of target gas pulses was generated for 10 minutes followed by synthetic air pulse. This procedure was continued until a stable baseline was observed after alternate pulses. This was followed by the experimental sequence of pulses with data recording. Each sensor was tested at different temperatures ranging from100^oC to 280^oC at 50^oC intervals under various concentrations of H_2 and ethanol, determining the optimum operating temperature by comparing the response amplitude achieved. Finally two full range tests for each sensor were performed at the optimum operating temperature for each gas. The response amplitude (S) of the films is defined as the ratio:

$$S = \frac{R_{air} - R_{gas}}{R_{gas}} \qquad (1)$$

where R_{air} is the resistance in air under stationary conditions and R_{gas} represents the resistance after the sensor is exposed to the target gas during a definite time. Equation (1) can be applied for n-type material such as WO_3 and reducing gases such as H_2 and C_2H_5OH.

3. Results and Discussions

3.1 Thin Film Analysis

The GIXRD patterns of WO_3 films before and after annealing (at 300°C and 400°C) are shown in Figure 1. The as-deposited and 300°C annealed films do not show any diffraction pattern which indicates that the as-deposited WO_3 film is highly amorphous and annealing the WO_3 film at 300°C for 2 hours in air did not induce significant crystallinity in the film. However, after annealing at 400°C, significant crystallinity is observed in the film, indicated by appearance of diffraction peaks in GIXRD pattern. The peaks obtained at 2θ = 24.112°, 28.538°, 34.361°, 41.615°, 49.843°, 55.684°, 61.941° are closely related to monoclinic WO_3 phase [44]. It should be noted that the lattice parameters of orthorhombic WO_3 phase are very similar to monoclinic phase, and thus these two phases cannot be distinguished within the accuracy of GIXRD data. It is reported that the two intense peaks observed at 2θ=24.278° and 34.117°, belong to (2 0 0) and (2 2 0) monoclinic planes of WO_3 corresponding to d=3.663° and 2.626 Å, respectively [45]. The lattice parameters were found to be a = 7.375 Å, b = 7.375 Å and c = 3.903 Å and its unit cell volume is about 212.38 $Å^3$.

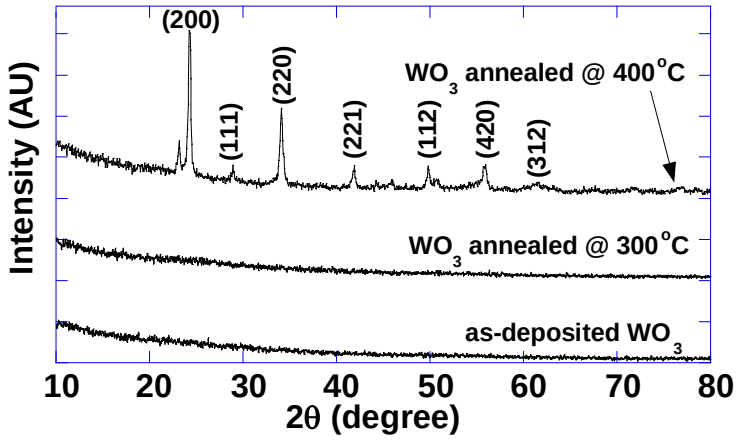

Figure 1. GIXRD spectra of as-deposited and annealed nanostructured WO_3 thin films.

Figure 2 (a,b) shows the surface topography of the as-deposited and 300°C annealed WO_3 films obtained using AFM semicontact mode. The topography of the as-deposited film (Figure 2a) reveals a nanostructured surface made up of particle clusters with 0.5 nm roughness and a mean size of 13 nm. It appears that the high evaporation rate during film deposition resulted in highly amorphous films made up of clusters (particles). Annealing of the as-deposited WO_3 film at 300°C for 2 hours in air slightly reduced the particle size from 13 nm to 10 nm without significant change in roughness (Figure 2b). Annealing of the WO_3 films at 400°C in air for 2 hours resulted in very fine grains of size 5 nm as shown from the TEM image in Figure 2c. The nucleation, successive grain growth and coalescence during annealing at 400°C transformed the clusters into smaller grains.

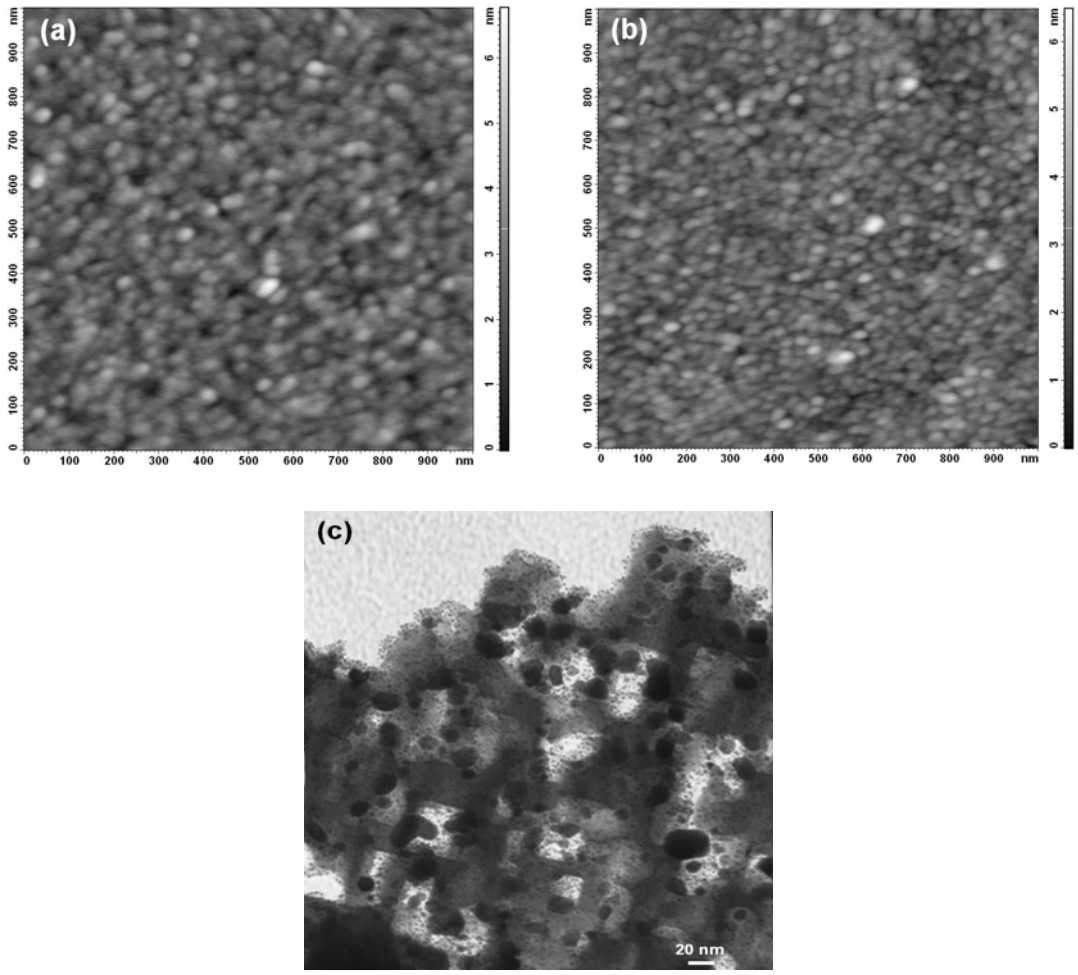

Figure 2. AFM semicontact mode images of (a) as-deposited, (b) 300°C annealed WO_3 and (c) TEM image of 400°C annealed nanostructured WO_3 films.

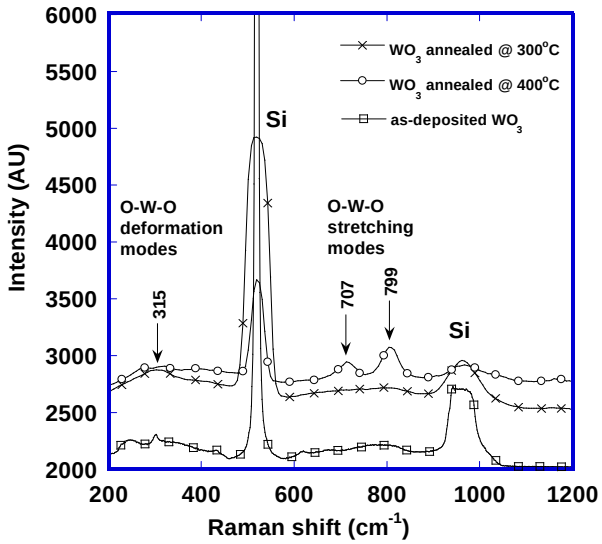

Figure 3: Raman spectra of as-deposited and annealed nanostructured WO_3 films.

The Raman spectra of as-deposited and annealed WO_3 films are shown in Figure 3. Two characteristic Raman bands are associated with WO_3. The first band, associated with O-W-O bending vibration modes, lies between 200 and 500 cm^{-1}. The second band lies in the range 600-1000 cm^{-1} and is associated with O-W-O stretching vibration modes. The as-deposited WO_3 film exhibited two weak and broad Raman bands centered at 315 cm^{-1} and 799 cm^{-1}, respectively. These features are characteristic of amorphous materials and are usually assigned bending and stretching vibration modes of the monoclinic WO_3 phase [46]. The amorphous nature of as-deposited WO_3 films is also confirmed by GIXRD analysis. The film annealed at 300^oC also appears to be amorphous with a slight broadening of the peak at 315 cm^{-1}. However, the appearance of two O-W-O stretching modes peaks at 707 cm^{-1} and 799 cm^{-1} [47] confirm the increase of crystallinity of the WO_3 film after annealing at 400^oC, confirming the results from GIXRD analysis. Raman analysis shows that films annealed at 300^oC are still amorphous. Annealing at a higher temperature of 400^oC induced significant crystallinity in the film.

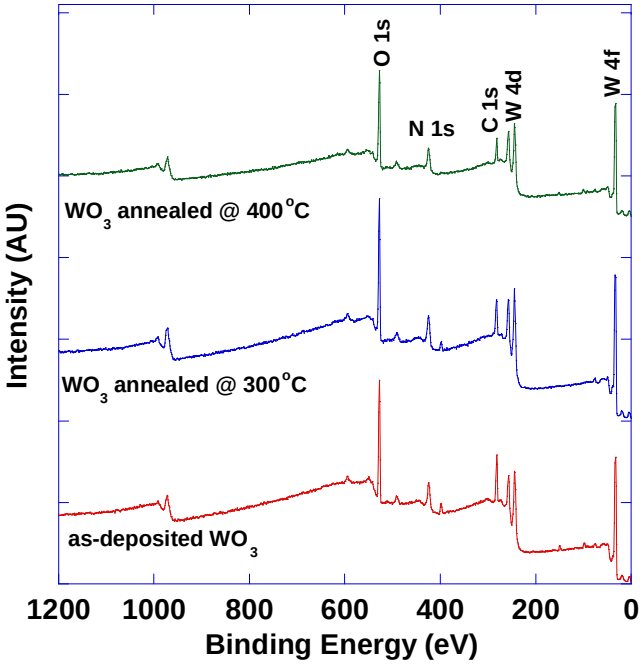

Figure 4: XPS wide survey scans of as-deposited and annealed nanostructured WO_3 films.

Figure 4 shows the XPS spectra obtained from wide survey scans on the surface of as-deposited and annealed WO_3 films between binding energies 0 and 1200 eV. Peaks of O, N, C and W are observed in all the films. Presence of carbon and nitrogen on the surface is attributed to atmospheric contamination. The C peak measured at binding energy of 284.80 eV coincides with literature reported [48] C 1s binding energy and is used as energy reference for the XPS measurements. It can be observed from Figure 4 that with increasing annealing temperature, the intensity of O and C peaks drops slightly, indicating desorption of surface contamination upon annealing.

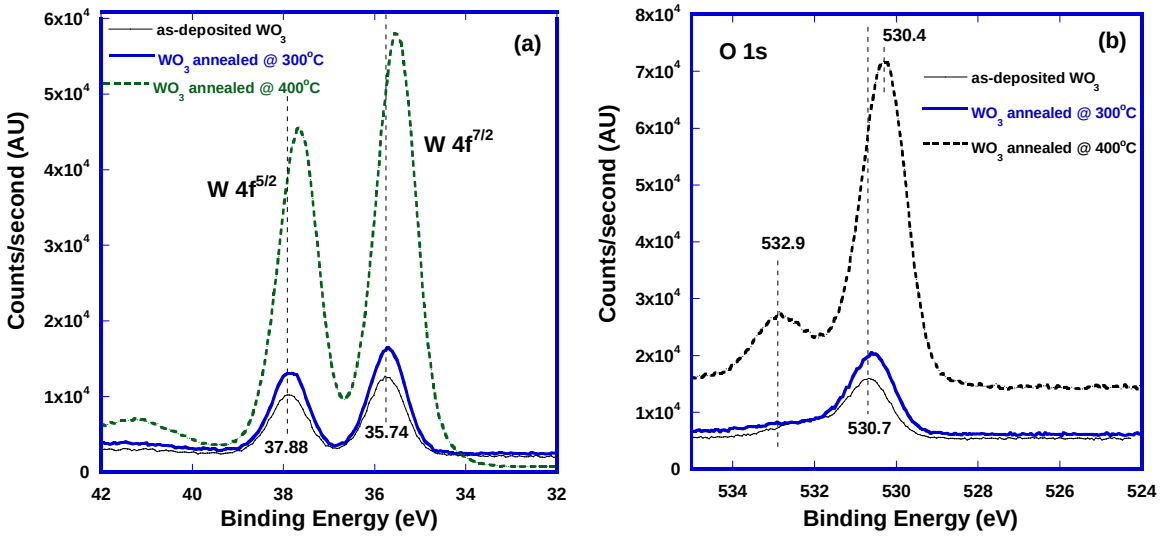

Figure 5: High resolution XPS core level W 4f (a) and O 1s (b) spectra of as-deposited and annealed nanostructured WO_3 films.

Figure 5 shows the high resolution core level W 4f and O 1s spectra of WO_3 films. For the as-deposited WO_3 film, the core level spectra of W 4f are observed at binding energy E_b of 35.74 eV and 37.88 eV corresponding to W $4f^{7/2}$ and W $4f^{5/2}$, respectively (Figure 5a). The literature reported E_b value for W $4f^{7/2}$ is 35.8 eV [49]. The measured value of 35.74 eV is in good agreement with those of WO_3 powder, electron beam evaporated and electrodeposited WO_3 films [50]. The W 4f peak shapes get sharper with increasing annealing temperature, which indicates that the surface becomes cleaner due to desorption of surface contaminants by annealing. The broadening of peaks is associated with change in stoichiometry of the sample surface, with the formation of different oxides such as WO_2 or WO [51]. The W $4f^{7/2}$ peak of metallic tungsten is located at 31.50 eV [52]. The W $4f^{7/2}$ peaks located at +4.5, +3 and +1.5 from the metallic tungsten W $4f^{7/2}$ peak are attributed to W^{6+}, W^{5+} and W^{4+} electronic states, respectively [53]. No significant change in the W $4f^{7/2}$ binding energy is observed when the WO_3 film is annealed at 300°C. However, an annealing at 400°C shifts the W $4f^{7/2}$ peak by 0.3 eV down to 35.44, indicating the presence of mixed tungsten states [54]. This can be explained by considering that, if an oxygen vacancy exists in the film, the electronic density near its adjacent W atom increases, creating a larger screening, which lowers the 4f level binding energy [55]. Oxygen vacancies play an important role as adsorption sites for gaseous species and eventually a minor shift of the binding energy may imply greatly enhanced gas sensitivity [56].

The O 1s core level high resolution spectra of as-deposited and annealed WO_3 films (Figure 5b) shows E_b of 530.7 eV for as-deposited WO_3 film. The main maxima does not change upon annealing at 300°C, while annealing at 400°C lowers the binding energy E_b by 0.3 eV, as in the W 4f peak, pointing

to a shift of the Fermi level, which corresponds to a band bending due to the desorption of surface contaminants during annealing at 400°C [57]. A small shoulder centered at about 532.9 eV is observed in the as-deposited and 300°C annealed films. This shoulder transforms into a peak when the film is annealed at 400°C. Such feature is a characteristic of substoichiometric monoclinic tungsten oxides [58]. The formation and increasing intensity of this feature is in the sequence $WO_3 \rightarrow WO_2$. XPS analysis reveals that after annealing at 400°C, the film surface is free from contamination and has mixed W states. This indicates the presence of oxygen vacancies in the film, which is highly beneficial for gas sensing.

3.2 Gas sensor characterization

3.2.1 Response of WO_3 thin films towards hydrogen

Nanostructured WO_3 thin film based gas sensors were characterized for their sensing performance towards various concentrations of H_2 in the temperature range 100°C-280°C. The as-deposited WO_3 film did not show any response towards H_2 in the measured temperature range (100°C-280°C) and concentrations. This film is found unsuitable for gas sensing due to the highly amorphous nature of the film. Some little response of the as-deposited film to H_2 was observed at about 280°C (Figure 6a) when the WO_3 film is annealed at 300°C. It is noticeable that the baseline and the dynamic resistance of this film are not stable (Figure 6a). The 400°C annealed film shows significant response towards H_2 with a stable dynamic resistance curve (Figure 6b), which is attributed to an improved crystalline properties of the film.

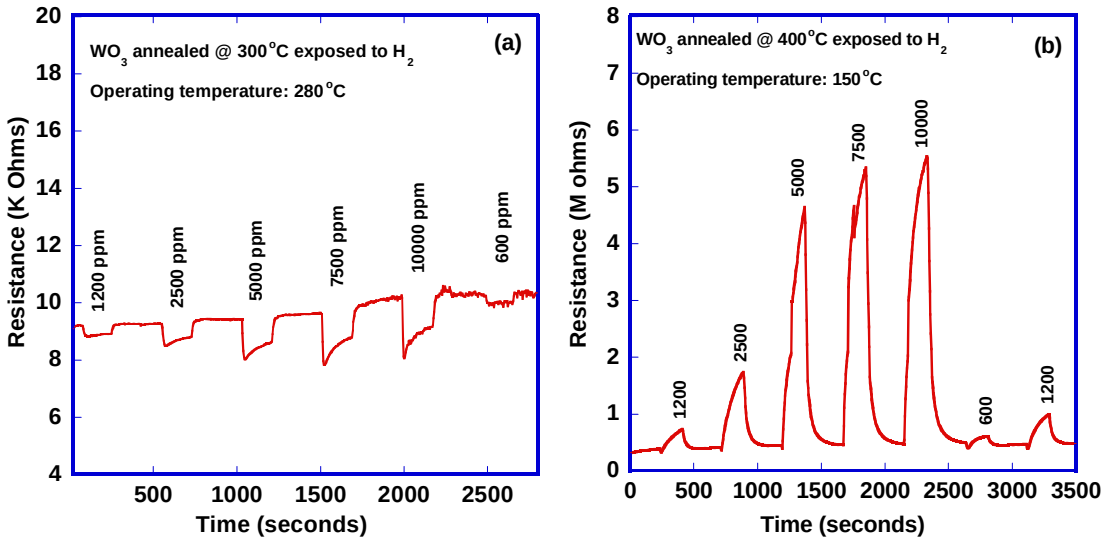

Figure 6: Dynamic resistance curve of nanostructured WO_3 thin films annealed at 300°C (a) and 400°C (b) upon exposure to H_2.

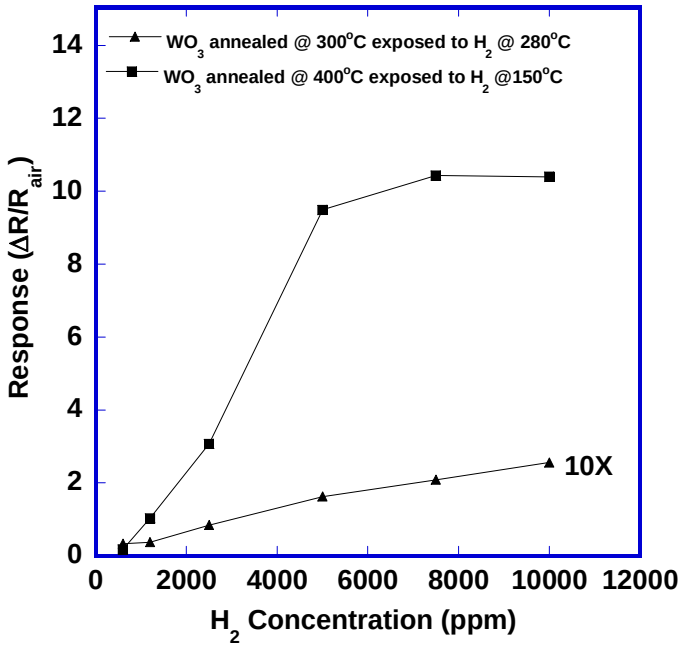

Figure 7: Response upon exposure to H_2 of nanostructured WO_3 thin films. Triangles: film annealed at 300˚C, response (x10) measured at 280˚C. Squares: film annealed at 400°C (b), response measured at 150 ˚C.

The 300°C annealed WO_3 film shows maximum response amplitude of 0.3 to 10,000 ppm H_2 at 280°C (Figure 7). Maximum response amplitude of 10 is obtained at a much lower operating temperature (150°C) from the 400°C annealed film (Figure 7). However, it must be noticed that in the latter case the response dynamics are very slow. For 10,000 ppm H_2 response and recovery times of 40 s and 44 s respectively, are observed for the 300°C annealed film, whereas response and recovery times of 140 s and 80 s, are observed for the 400°C annealed WO_3 film. This is not surprising as the gas dynamics slow down at lower operating temperature[59].

WO_3 is an n-type semiconductor material and commonly operates as gas sensor in the temperature range 200°C-500°C [38]. When it is exposed to a reducing gas such as H_2, the oxygen adsorbates on the film surface interact with the gas and release electrons back to the film, causing a drop in film resistance. This behavior is observed for the 300°C annealed WO_3 film when exposed to H_2 at 280°C. However the opposite behavior (i.e. an increase in resistance) is observed for the 400°C annealed WO_3 film upon exposure to H_2 at 150°C. Such behavior cannot be explained by merely considering the microstructural properties such as grain size and porosity of the film. In polycrystalline materials, surface barriers are formed at the intergranular surfaces which electrons have to overcome for taking part in the conduction mechanism. The height of surface barrier depends on concentration of charge carriers (oxygen adsorbates) at the surface, therefore, overall resistance changes can be correlated with

changes in surface band bending. The overall resistance and hence, surface band bending increase exponentially when polycrystalline WO_3 surface is exposed to increasing concentrations of oxygen [60]. The observed behavior in the 400°C annealed WO_3 film exposed to H_2 at operating temperature of 150°C might arise from various forms of oxygen adsorbates (O^-, O_2^- and O^{2-}) on WO_3 surface, which depend on temperature. At 150°C, the most dominant form of adsorbed oxygen is O_2^- [61]. Upon exposure to H_2, the O_2^- species dissociates into O^- with the formation of water, as per the following equation.

$$H_2 + O_2^- \rightarrow H_2O + O^- \qquad (2)$$

At 150°C, the rate of water desorption from the surface is higher than rate of water formation [62]. In situ Raman analysis of WO_3 films annealed at 300°C and 400°C show that rate of water desorption above 100°C was much faster than the rate of water formation on the film surface when WO_3 film was exposed to H_2 [62]. The high concentration range of H_2 (600 ppm – 10000 ppm) produces more O^- species on the surface, leading to increase in surface barrier height, consequently increasing the resistance. Hence, this can be a reason why an increase in resistance was observed at lower operating temperature. The high response observed for the 400°C annealed WO_3 film towards H_2 at 150°C is attributed to its highly crystalline nature, very small grain size (5 nm) and a porous structure (see Figure 1). The film is also composed of mixed W states, as observed in XPS analysis, resulting in increased number of oxygen vacancies on the surface, when compared to as-deposited or the 300°C annealed film.

No significant difference in porosity was observed of the annealed films as compared to the as-deposited film. Interaction of H_2 with Pt might be possible through the pores in the film as well as exposed portions of the Pt electrode. However, no response to H_2 was observed in the case of as-deposited WO_3 films, little response from the 300°C annealed film and good response from 400°C annealed film. This indicates that the response to these gases arises mainly from the improved properties (example: crystallinity and oxygen vacancies) of the film achieved by annealing at 400°C.

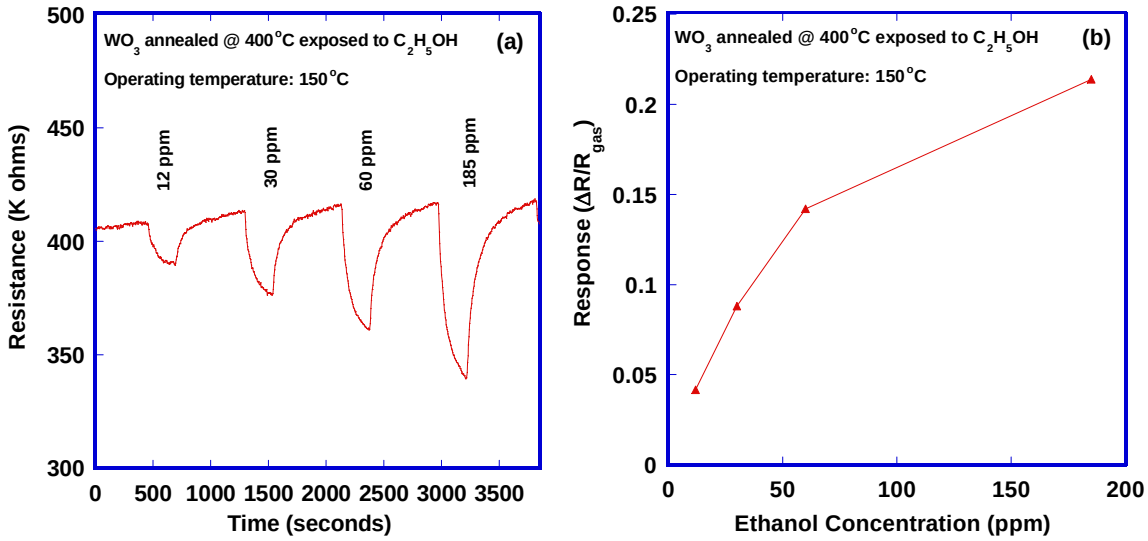

Figure 8: Dynamic resistance curve (a) and Response (b) of nanostructured WO_3 film annealed at 400°C for 2 hours in air, exposed to C_2H_5OH.

3.2.2 Response of WO_3 thin films towards ethanol

The as-deposited and 300°C annealed WO_3 films show no response towards ethanol in the measured temperature range and concentrations and found unsuitable for ethanol sensing. This may be attributed to the amorphous nature of the films. The dynamic resistance curve and response of 400°C annealed WO_3 film exposed to ethanol at 150°C are shown in Figure 8. The film exhibits a stable baseline resistance (Figure 8a), owing to its crystalline properties. The response amplitude increased with increasing ethanol concentration, reaching 0.2 for 185 ppm ethanol (Figure 8b). The response and recovery times for 185 ppm ethanol are found to be 180 s and 288 s, respectively.

The dominant oxygen species on the film surface at 150°C is O_2^-, the conduction mechanism takes place by the following reaction:

$$C_2H_5OH + O_2^- \rightarrow CH_3COOH + e^- \qquad (3)$$

The above reaction increases the concentration of electrons, which decreases the surface band bending, resulting in drop in resistance. Hence, a decrease in resistance is observed upon exposure to ethanol. With increasing concentration of ethanol, a further drop in resistance is expected, which is confirmed by the dynamic response (Figure 8a). The response of the 400°C annealed WO_3 film at 150°C is much higher to H_2 (S=10) than ethanol (S=0.2). Hydrogen molecule is small compared to ethanol and can easily diffuse through the porous film and interact with more surface area, hence, higher response may be achieved. The gas sensing performance depends on a number of factors which include grain size, porosity, oxygen vacancies and the type of adsorbates on the film surface. In the present study, the

400°C annealed films are found to be highly porous and crystalline with very small grain size of 5 nm. Moreover, these films contain high number of vacancies. All these factors have contributed significantly towards improved sensing performance of these films to hydrogen and ethanol at a lower operating temperature of 150°C.

4. Conclusions

Highly amorphous nanostructured WO_3 thin films with cluster of particles have been obtained at high deposition rate of 35 nm/second using thermal evaporation. Post deposition annealing of the as-deposited films at 300°C for 2 hours in air didn't show crystalline characteristics of the film. However, annealing at 400°C for 2 hours in air transformed these clusters into very fine crystalline grains of about 5 nm, and induced mixed tungsten states (W^{6+}, W^{5+} and W^{4+}) in the films. The WO_3 film annealed at 300°C showed little response to H_2 at an operating temperature of 280°C and no response towards C_2H_5OH in the temperature range 100°C-280°C. However, the film annealed at 400°C showed high response to H_2 and C_2H_5OH with maximum response amplitude of S=10 and S=0.2, respectively at an operating temperature of 150°C. The high film porosity with significant oxygen vacancies and very small crystalline grains achieved by annealing at 400°C greatly influenced the hydrogen and ethanol sensing performance of the thermally evaporated WO_3 sensor at lower operating temperature of 150°C.

Acknowledgements

The authors would like to acknowledge Nina DeCaritat from Australian National University and Dr. Barry Wood from University of Queensland for providing their facility and support during this research. This research was carried out at Queensland University of Technology and RMIT, and was funded by the Queensland Government through the NIRAP program "Solar Powered Nanosensors".

References

[1] R. Sivakumar, R. Gopalakrishnan, M. Jayachandran, C. Sanjeeviraja, Preparation and characterization of electron beam evaporated WO_3 thin films, Optical Materials, 29 (2007) 679-687.
[2] W. Smith, Z.Y. Zhang, Y.P. Zhao, Structural and optical characterization of WO_3 nanorods/films prepared by oblique angle deposition, Journal of Vacuum Science and Technology B, 25 (2007) 1875.
[3] L. Lietti, J.L. Alemany, P. Forzatti, G. Busca, G. Ramis, E. Giamello, F. Bregani, Reactivity of V_2O_5-WO_3/TiO_2 catalysts in the selective catalytic reduction of nitric oxide by ammonia, Catalysis Today, 29 (1996) 143-148.
[4] C.G. Granqvist, Handbook of Inorganic Electronic Materials, Elsevier, Amsterdam, 1995.
[5] A. Ponzoni, E. Comini, M. Ferroni, G. Sberveglieri, Nanostructured WO_3 deposited by modified thermal evaporation for gas-sensing applications, Thin Solid Films, 490 (2005) 81-85.

[6] R. Boulmani, M. Bendahan, C. Lambert-Mauriat, M. Gillet, K. Aguir, Correlation between rf-sputtering parameters and WO_3 sensor response towards ozone, Sensors and Actuators B: Chemical, 125 (2007) 622-627.
[7] H.-H. Lu, Effects of oxygen contents on the electrochromic properties of tungsten oxide films prepared by reactive magnetron sputtering, Journal of Alloys and Compounds, 465 (2008) 429-435.
[8] T. Siciliano, A. Tepore, G. Micocci, A. Serra, D. Manno, E. Filippo, WO_3 gas sensors prepared by thermal oxidization of tungsten, Sensors and Actuators B: Chemical, 133 (2008) 321-326.
[9] A. Antonaia, T. Polichetti, M.L. Addonizio, S. Aprea, C. Minarini, A. Rubino, Structural and optical characterization of amorphous and crystalline evaporated WO_3 layers, Thin Solid Films, 354 (1999) 73-81.
[10] A. Hoel, L.F. Reyes, P. Heszler, V. Lantto, C.G. Granqvist, Nanomaterials for environmental applications: novel WO_3-based gas sensors made by advanced gas deposition, Current Applied Physics, 4 (2004) 547-553.
[11] Y.-G. Choi, G. Sakai, K. Shimanoe, N. Miura, N. Yamazoe, Wet process-prepared thick films of WO_3 for NO_2 sensing, Sensors and Actuators B: Chemical, 95 (2003) 258-265.
[12] N. Barsan, M. Schweizer-Berberich, W. Göpel†, Fundamental and practical aspects in the design of nanoscaled SnO_2 gas sensors: a status report, Fresenius' Journal of Analytical Chemistry, 365 (1999) 287-304.
[13] X. Wang, S.S. Yee, W.P. Carey, Transition between neck-controlled and grain-boundary-controlled sensitivity of metal-oxide gas sensors, Sensors and Actuators B: Chemical, 25 (1995) 454-457.
[14] M. Ahsan, T. Tesfamichael, A. Ponzoni, G. Faglia, Sensing Properties of E-Beam Evaporated Nanostructured Pure and Iron-Doped Tungsten Oxide Thin Films, Sensor Letters, 9 (2011) 759-762.
[15] D.-S. Lee, S.-D. Han, J.-S. Huh, D.-D. Lee, Nitrogen oxides-sensing characteristics of WO_3-based nanocrystalline thick film gas sensor, Sensors and Actuators B: Chemical, 60 (1999) 57-63.
[16] D.-S. Lee, J.-W. Lim, S.-M. Lee, J.-S. Huh, D.-D. Lee, Fabrication and characterization of micro-gas sensor for nitrogen oxides gas detection, Sensors and Actuators B: Chemical, 64 (2000) 31-36.
[17] D.J. Smith, J.F. Vatelino, R.S. Falconer, E.L. Wittman, Stability, sensitivity and selectivity of tungsten trioxide films for sensing applications, Sensors and Actuators B: Chemical, 13 (1993) 264-268.
[18] M. Stankova, X. Vilanova, J. Calderer, E. Llobet, J. Brezmes, I. Gràcia, C. Cané, X. Correig, Sensitivity and selectivity improvement of rf sputtered WO_3 microhotplate gas sensors, Sensors and Actuators B: Chemical, 113 (2006) 241-248.
[19] A. Qurashi, E.M. El-Maghraby, T. Yamazaki, Y. Shen, T. Kikuta, A generic approach for controlled synthesis of In2O3 nanostructures for gas sensing applications, Journal of Alloys and Compounds, 481 (2009) L35-L39.
[20] A. Qurashi, E.M. El-Maghraby, T. Yamazaki, T. Kikuta, Catalyst supported growth of In2O3 nanostructures and their hydrogen gas sensing properties, Sensors and Actuators B: Chemical, 147 48-54.
[21] C.S. Rout, M. Hegde, C.N.R. Rao, H_2S sensors based on tungsten oxide nanostructures, Sensors and Actuators B: Chemical, 128 (2008) 488-493.
[22] D.-S. Lee, K.-H. Nam, D.-D. Lee, Effect of substrate on NO_2-sensing properties of WO_3 thin film gas sensors, Thin Solid Films, 375 (2000) 142-146.
[23] M. Penza, M.A. Tagliente, L. Mirenghi, C. Gerardi, C. Martucci, G. Cassano, Tungsten trioxide (WO_3) sputtered thin films for a NOx gas sensor, Sensors and Actuators, B: Chemical, 50 (1998) 9-18.
[24] E. Rossinyol, A. Prim, E. Pellicer, J. Rodríguez, F. Peiró, A. Cornet, J.R. Morante, B. Tian, T. Bo, D. Zhao, Mesostructured pure and copper-catalyzed tungsten oxide for NO_2 detection, Sensors and Actuators B: Chemical, 126 (2007) 18-23.
[25] H. Xia, Y. Wang, F. Kong, S. Wang, B. Zhu, X. Guo, J. Zhang, Y. Wang, S. Wu, Au-doped WO_3-based sensor for NO_2 detection at low operating temperature, Sensors and Actuators B: Chemical, 134 (2008) 133-139.

[26] S. Vallejos, V. Khatko, J. Calderer, I. Gracia, C. Cané, E. Llobet, X. Correig, Micro-machined WO_3-based sensors selective to oxidizing gases, Sensors and Actuators B: Chemical, 132 (2008) 209-215.
[27] Y. Shen, T. Yamazaki, Z. Liu, D. Meng, T. Kikuta, N. Nakatani, Influence of effective surface area on gas sensing properties of WO_3 sputtered thin films, Thin Solid Films, 517 (2009) 2069-2072.
[28] M.H. Yaacob, M. Breedon, K. Kalantar-zadeh, W. Wlodarski, Absorption spectral response of nanotextured WO_3 thin films with Pt catalyst towards H_2, Sensors and Actuators B: Chemical, 137 (2009) 115-120.
[29] V. Khatko, G. Gorokh, A. Mozalev, D. Solovei, E. Llobet, X. Vilanova, X. Correig, Tungsten trioxide sensing layers on highly ordered nanoporous alumina template, Sensors and Actuators, B: Chemical, 118 (2006) 255-262.
[30] A. Labidi, E. Gillet, R. Delamare, M. Maaref, K. Aguir, Ethanol and ozone sensing characteristics of WO_3 based sensors activated by Au and Pd, Sensors and Actuators, B: Chemical, 120 (2006) 338-345.
[31] A. Labidi, C. Lambert-Mauriat, C. Jacolin, M. Bendahan, M. Maaref, K. Aguir, dc and ac characterizations of WO_3 sensors under ethanol vapors, Sensors and Actuators, B: Chemical, 119 (2006) 374-379.
[32] M. Sriyudthsak, S. Supothina, Humidity-insensitive and low oxygen dependence tungsten oxide gas sensors, Sensors and Actuators, B: Chemical, 113 (2006) 265-271.
[33] A.Y. Lyashkov, A.S. Tonkoshkur, V.O. Makarov, Gas sensing properties of WO_3-based ceramics to ethanol vapors, Sensors and Actuators B: Chemical, 148 (2010) 1-5.
[34] C. Zhang, A. Boudiba, C. Navio, C. Bittencourt, M.-G. Olivier, R. Snyders, M. Debliquy, Highly sensitive hydrogen sensors based on co-sputtered platinum-activated tungsten oxide films, International Journal of Hydrogen Energy, 36 (2011) 1107-1114.
[35] A. Boudiba, C. Zhang, C. Navio, C. Bittencourt, R. Snyders, M. Debliquy, Preparation of highly selective, sensitive and stable hydrogen sensors based on Pd-doped tungsten trioxide, Procedia Engineering, 5 (2010) 180-183.
[36] E. Comini, L. Pandolfi, S. Kaciulis, G. Faglia, G. Sberveglieri, Correlation between atomic composition and gas sensing properties in tungsten-iron oxide thin films, Sensors and Actuators B: Chemical, 127 (2007) 22-28.
[37] V. Khatko, S. Vallejos, J. Calderer, E. Llobet, X. Vilanova, X. Correig, Gas sensing properties of WO_3 thin films deposited by rf sputtering, Sensors and Actuators B: Chemical, 126 (2007) 400-405.
[38] P.G. Su, T.T. Pan, Fabrication of a room-temperature NO_2 gas sensor based on WO_3 films and WO_3/MWCNT nanocomposite films by combining polyol process with metal organic decomposition method, Materials Chemistry and Physics, 125 (2011) 351-357.
[39] B. Yuliarto, I. Honma, Y. Katsumura, H. Zhou, Preparation of room temperature NO2 gas sensors based on W- and V-modified mesoporous MCM-41 thin films employing surface photovoltage technique, Sensors and Actuators B: Chemical, 114 (2006) 109-119.
[40] M.K. Verma, V. Gupta, A highly sensitive SnO2â€“CuO multilayered sensor structure for detection of H2S gas, Sensors and Actuators B: Chemical, 166â€“167 378-385.
[41] J.Z. Ou, M.Z. Ahmad, K. Latham, K. Kalantar-zadeh, G. Sberveglieri, W. Wlodarski, Synthesis of the nanostructured WO3 via anodization at elevated temperature for H2 sensing applications, Procedia Engineering, 25 247-251.
[42] L.G. Teoh, Y.M. Hon, J. Shieh, W.H. Lai, M.H. Hon, Sensitivity properties of a novel NO2 gas sensor based on mesoporous WO3 thin film, Sensors and Actuators B: Chemical, 96 (2003) 219-225.
[43] Z. Liu, T. Yamazaki, Y. Shen, T. Kikuta, N. Nakatani, Influence of annealing on microstructure and NO2-sensing properties of sputtered WO3 thin films, Sensors and Actuators B: Chemical, 128 (2007) 173-178.
[44] J. Diaz-Reyes, F.-M. J.E., J.M. Gutierrez-Arias, M.M. Morin-Castillo, H. Azucena-Coyotecatl, M. Galvan, P. Rodriguez-Fragoso, A. Mendez-Lopez, Optical and structural properties of WO_3 as a

function of the annealing temperature, in: O. Frazao (Ed.) 3rd WSEAS International Conference on Sensors and Signals (SENSIG'10), WSEAS Press, Portugal, 2010, pp. 99-104.
[45] S.C. Moulzolf, L.J. LeGore, R.J. Lad, Heteroepitaxial growth of tungsten oxide films on sapphire for chemical gas sensors, Thin Solid Films, 400 (2001) 56-63.
[46] K.J. Lethy, D. Beena, R.V. Kumar, V.P.M. Pillai, V. Ganesan, V. Sathe, Structural, optical and morphological studies on laser ablated nanostructured WO_3 thin films, Applied surface Science, 254 (2008) 2369-2376.
[47] E. Salje, K. Viswanathan, Physical properties and phase transitions in WO_3, Acta Crystallographica A, 31 (1975) 356-359.
[48] K.G. Saw, D. Plessis J, The X-ray photoelectron spectroscopy C 1s Diamond Peak of chemical vapor deposition diamond from a sharp interfacial structure, Materials Letters, 58 (2004) 1344-1348.
[49] J.F. Morar, F.J. Himpsel, G. Hughes, J.L. Jordan, F.R. McFeely, G. Hollinger, High resolution photoemission investigation: The oxidation of W, Journal of Vacuum Science and Technology A: Vacuum, Surfaces and Films, 3 (1985) 1477-1480.
[50] J.N. Yao, P. Chen, A. Fujishima, Electrochromic behavior of electrodeposited tungsten oxide thin films, Journal of Electroanalytical Chemistry, 406 (1996) 223-226.
[51] T.G.G. Maffeis, M.W. Penny, R.J. Cobley, E. Comini, G. Sberveglieri, S.P. Wilks, XPS characterization of vacuum annealed nanocrystalline WO_3 films, e-Journal of Surface Science and Nanotechnology, 7 (2009) 319-322.
[52] M. Regragui, M. Addou, A. Outzourhit, J.C. Bernéde, E. El Idrissi, E. Benseddik, A. Kachouane, Preparation and characterization of pyrolytic spray deposited electrochromic tungsten trioxide films, Thin Solid Films, 358 (2000) 40-45.
[53] G. Hollinger, in, Thesis, Universite Claude Bernad, Lyon, 1976.
[54] S. Santucci, C. Cantalini, M. Crivellari, L. Lozzi, L. Ottaiano, M. Passacantando, X-ray photoemission spectroscopy and scanning tunneling spectroscopy study on thermal stability of WO_3 thin films, Journal of Vacuum Science and Technology, 18 (2000) 1077.
[55] C.G. Granqvist, CRC Handbook of Solid State Electrochemistry, CRC Press, Inc., Cleveland and Ohio, 1997.
[56] N. Yamazoe, New approaches for improving semiconductor gas sensors, Sensors and Actuators B: Chemical, 5 (1991) 7-19.
[57] T.G.G. Maffeis, D. Yung, L. LePennec, M.W. Penny, R.J. Cobley, E. Comini, G. Sberveglieri, S.P. Wilks, STM and XPS characterisation of vacuum annealed nanocrystalline WO_3 films, Surface Science, 601 (2007) 4953-4957.
[58] O.Y. Khyzhun, XPS, XES and XAS studies of the electronic structure of tungsten oxides, Journal of Alloys and Compounds, 305 (2000) 1-6.
[59] J. Polleux, A. Gurlo, N. Barsan, U. Weimar, M. Antonietti, M. Niederberger, Template-free synthesis and assembly of single-crystalline tungsten oxide nanowires and their gas-sensing properties, Angewandte Chemie-International Edition, 45 (2006) 261-265.
[60] C.E. Simion, A. Tomescu-Stanoiu, Differences in the gas sensing properties readout with N and P-type MOX materials, in: International Semiconductor Conferences, 2011.
[61] W. Gopel, K.D. Schierbaum, SnO_2 sensors: current status and future prospects, Sensors and Actuators B, 26 (1995) 1.
[62] J.Z. Ou, M.H. Yaacob, M. Breedon, H.D. Zheng, J.L. Campbell, K. Latham, J.d. Plessis, W. Wlodarski, K. Kalantar-zadeh, In situ Raman spectroscopy of H_2 interaction with WO_3 films, Physical Chemistry Chemical Physics, 13 (2011) 7330-7339.

Authors Biographies

Mr. Mohammed Ahsan

Mr. Mohammed Ahsan received his PhD in Materials Engineering and Nanotechnology from Queensland University of Technology (2012). He has an excellent research experience and publication track record in the field of materials science and engineering. He served as a Lecturer at King Fahd University of Petroleum & Minerals, Saudi Arabia from 2003-2008 and has been involved in a number of national and international projects. His research interests include nanomaterials, nanostructured thin films and nano characterization. His has over 25 publications with focus on material testing, microstructural characterization and development of thin films.

Dr. Tuquabo Tesfamichael

Dr. Tuquabo Tesfamichael received his Ph.D. in Solid State Physics in 2000 from Uppsala University, Sweden. He is serving as academic teaching and research staff at Queensland University of Technology from 2003. He has received over $2 million in research funding and awards from external competitive grants. His research has been focused on the development of metal oxide nanomaterials, thin film coatings, surface modification and thin film characterisations for solar cells and gas sensing applications. He has published over 30 refereed articles in high impact and widely read journals.

Professor John Bell

Professor John Bell is the Assistant Dean Research at the Queensland University of Technology, and has an excellent research funding and publication track record. He has a wealth of experience in the synthesis of thin film electronic and optical materials, including diamond-like carbon materials and dye-sensitised titania solar cells. He also has experience in modification of materials by ion implantation and allied techniques, charge transport in photovoltaic devices, especially dye-sensitised cells, and optical phsyics. Prof. Bell has over 150 publications, the majority focussing on optical devices, and including research on photovoltaic module design for DSC cells and polymer solar cells.

Professor Wojtek Wlodarski

Professor Wojtek Wlodarski has worked in the areas of sensor technology and instrumentation for over 30 years. He has published 4 books and monographs, over 400 papers and holds 29 patents. He is a

professor at RMIT University, Melbourne, Australia, and heads the Sensor Technology Laboratory at the School of Electrical and Computer Engineering.

Asociate Professor Nunzio Motta

Associate Professor Nunzio Motta has obtained his Laura in Physics in 1981 (Università La Sapienza – Roma) and his PhD in Physics in 1986 (Scuola Normale Superiore - Pisa). He is currently leading research at QUT in solar energy and environmental nanotechnology, developing new polymer solar cells and solar powered nanosensors. He is internationally recognized in the field of material science, with over 20 years experience in growth and characterization of nanostructures, Scanning Tunnelling Microscopy and Atomic Force Microscopy. Nunzio has obtained several visiting positions in various research institutions across Europe, published more than 110 papers in material science and surface physics and led many international research projects in the area of nanotechnology.